DALTON

Gas-phase metal sulfide cluster anions *

Keith Fisher, Ian Dance, Gary Willett and MaNu Yi

School of Chemistry, University of New South Wales, Sydney 2052, Australia

The formation of metal sulfide cluster anions by laser ablation of solids has been examined for most of the first-row transition metals. Maps of the compositions of the clusters $[M_xS_y]^-$ show well defined continuous distributions of x *vs.* y for each metal, and the slope of each distribution is related to the position of the metal in the transition series. The 290 new molecular forms of metal sulfides range in size up to $[Cu_{45}S_{23}]^-$. Fourier-transform ion cyclotron resonance mass spectrometry revealed that the cluster anions have lifetimes of up to 100 s *in vacuo*. Experiments concentrating on the copper–sulfur anions showed their resistance to dissociation on energised collision with argon, and their general lack of reactivity, except with sulfur-containing reactants. In experiments designed to produce mixed-metal anions, cobalt has been shown to substitute for copper in many of the smaller anions. Geometrical structures and structural principles for the copper sulfide clusters are revealed by non-local density functional calculations.

Metal sulfides normally occur as non-molecular solids, or as clusters ligated by terminal heteroligands.[1] How then can molecular forms of binary metal sulfides be generated? In this discussion we describe results from our experimental and theoretical research programmes in gas-phase inorganic chemistry, which reveal the formation and properties of anionic clusters $[M_xS_y]^-$. These pristine molecular metal sulfides have no heteroligands, and are devoid of all the many external influences which occur in condensed phase systems. The further questions we are investigating include: (*a*) what are the compositions of the $[M_xS_y]^-$ which are stable, and how do they vary with the identity of M?; (*b*) what are the inherent stabilities of the $[M_xS_y]^-$, and how do they dissociate?; (*c*) how do the $[M_xS_y]^-$ behave with reactants able to function as ligands, as electron-transfer agents, and/or as proton-transfer reagents?; (*d*) what are the structures of the $[M_xS_y]^-$, and what geometrical factors confer stability?

In attempting to answer these questions we use laser ablation (LA) of binary transition-metal sulfides, and observe the anions formed using Fourier-transform ion cyclotron resonance (FTICR) mass spectrometry. Our laser ablation studies of metal sulfides have involved Ag_2S,[2] Ni_2S_3,[3] CuS, Cu_2S, and KCu_4S_3,[4] FeS,[5] CoS,[5] and V_2S_3, Cr_2S_3 and MnS; the last three systems are not yet published. A brief preliminary report of the generation and structure of some metal chalcogenide clusters has been published.[6] These laser ablation studies have yielded a large variety of stable metal sulfide cluster anions. For instance copper sulfide anions[4] have been identified up to $[Cu_{45}S_{23}]^-$, with two major series of anions of formulae $[Cu_{2n-1}S_n]^-$ and $[Cu_{2n-2}S_n]^-$ both appearing in the laser ablation spectra of several different copper sulfide compounds.

In the ion-trapping cell of the FTICR mass spectrometer we are able to store and treat these ions for several seconds, attesting to their inherent stability. Mass spectrometers using magnetic and electric sectors, or time-of-flight mass spectrometers, produce and observe ions in micro- or milli-seconds whereas in FTICR the observation of the ions has a detection window of at least 100 ms up to 100 s. One disadvantage of the techniques is that reactions can be studied only at very low pressure.

A range of source materials can be used for the generation of metal sulfide clusters by laser ablation, although the high vacuum required for good ion detection in FTICR does not allow the use of elemental sulfur, and the magnetic field precludes ferromagnetic samples. Many binary and ternary metal sulfides can be used, as can mixtures with metals, and mixtures of metal powder and selenium powder. We have observed that in general the distribution of metal chalcogenide clusters formed on laser ablation is largely independent of the sample ablated, and that similar copper selenide anions are formed on ablation of copper selenide or of a mixture of copper and selenium.[4]

Very few other studies have been made of gas-phase cluster *anions* involving transition metals. One recent investigation involved the Group 11 cluster anions,[7] M_n^-, prepared in a flowing afterglow ion source using a high-voltage cold-cathode d.c. discharge. These cluster anions were produced at relatively high pressures of 0.45 Torr, and their reactions with dioxygen and carbon monoxide were reported. Freiser and co-workers studied the reactions of bare metal anions with organic molecules including benzenethiol,[8] and of iron and cobalt anions[9] with sulfur compounds, producing metal polysulfide anions. Metal sulfide cluster anions have been produced and observed by other techniques, such as fast atom bombardment to form iron sulfide cubanoid ion clusters,[10] and secondary ion mass spectrometry of molecular nickel thiolates by Benninghoven and co-workers[11] to produce $[Ni_xS_y]^-$ anions related to those we produce. Freiser and co-workers[12] have investigated $[Cu_xO_y]^-$ clusters generated by laser ablation of CuO.

In our survey of the first-row transition-metal sulfides we have observed distributions of compositions $[M_xS_y]^-$ which are dependent on the identity of the metal M. The maps of composition appear to be related to the electron population of the metal, and so we question what happens when quite different metals have the opportunity to exist in the same cluster, and we have started to investigate mixed-metal systems to further our understanding of the formation and composition of the cluster anions.

The stability of the anions has been tested by collision-induced dissociation experiments, designed to measure the collisional energies needed to dissociate these anions, and the products of dissociation. Further information on the stabilities of the cluster anions can be obtained by investigation of their reactivity with gaseous reactants. Studies of other anions, for example the carbanions $[C_n]^-$,[13] have shown that anions are often unreactive with all but the most active reagents such as F_2.

* Basis of the presentation given at Dalton Discussion No. 1, 3rd–5th January 1996, University of Southampton, UK.

Non-SI units employed: Torr ≈ 133 Pa, bar = 10^5 Pa, eV ≈ 1.60×10^{-19} J.

Our recent report of the copper and silver cyanide cluster anions[14] also demonstrated the low reactivity of anions. We have discovered that some sulfur-containing reagents do react with anions, and these reagents have been investigated with copper–sulfur cluster anions. The initial reactivity experiments have concentrated on copper–sulfur clusters because a range of them can be isolated in the ion trap with good ion signal intensities, and can be observed for long reaction periods.

Geometrical and electronic structure are important facets of the chemistry of these new molecular forms of metal sulfides, and of their relationships to known condensed phase systems. There are as yet no spectroscopic or other experimental data which could inform discussion of the structures of the metal sulfide cluster anions, and therefore computational methods using density functional (DF) theory have been utilised to optimise postulated geometries and map the geometry–energy surfaces. Selected results on copper sulfide clusters are presented here.

Experimental

General

Three types of LA-FTICR experiment were undertaken.

(*a*) Generation and detection of cluster ions. These were carried out by laser ablation of pure metal sulfides, or mixtures of metal sulfides, or mixtures of cobalt metal and copper sulfides. They involved variation of the samples, the laser powers and the delays between ion formation and detection, in order to probe the requirements for anion formation.

(*b*) Collision-induced dissociation. Specific anions were selected and isolated by removal of the remainder of the ions from the mixture of anions formed after laser ablation. The selected anion was then translationally accelerated in the presence of an inert collision gas, argon, to assess its inherent stability and to examine any fragmentation pattern which could provide information about structure. Electron loss was tested by a similar experiment except that the collision gas was carbon tetrachloride.

(*c*) Reactions. A specific anion was selected and isolated in the presence of a gaseous reactant, and any products of reaction monitored after various time intervals.

Formation and observation

Experiments were carried out using a Spectrospin CMS-47 Fourier-transform ion cyclotron resonance mass spectrometer with a 4.7 T superconducting magnet. The ICR cell was cylindrical (r = 30 mm, l = 60 mm) with titanium end plates for electrostatic trapping of the ions in the magnetic field and equatorial titanium plates for radiofrequency excitation and detection of ions. A turbomolecular pump was used to keep the base pressure at 1×10^{-9} mbar. The sample to be ablated was pressed into a satellite probe tip which was placed at the end of the cell, in contact and flush with one of the trapping plates. The samples used were either pure metal sulfides, or physical mixtures of two metal sulfides, or mixtures of a metal powder with copper sulfide. The $[M_xE_y]^-$ anions were generated with a pulse from a Nd-YAG laser at 1064 nm, focused to a spot of 0.4 mm diameter, with a pulse duration of 8 ns and laser-power densities of 150 or 340 MW cm^{-2}. The plasma plume resulting from the laser ablation contained both positive and negative ions, but only negative ions were trapped by the negative potential on the trapping plates at the ends of the cell. The anions trapped in the cell were allowed a period of at least 100 ms (and up to 1 s) for collisional cooling, and were then excited into large cyclotron orbits by radiofrequency excitation, and detected by the time-dependent currents they induced on the detector plates. The resulting overlapping sine waves in the time domain were Fourier transformed to frequencies which were mass linearised to give the mass spectrum. Broad-band spectra involved the observation of anions formed over a wide range of masses, with lower and upper limits of 20 and 5000 daltons. In general, mass ranges were varied as necessary, with 100–1000 being the most common. In order to determine the compositions of anions accurately, narrow-band spectra were recorded over a small mass range generally covering only one manifold of isotopomers. Where a cluster involved only one isotopomer accurate mass measurements were made in the narrow-band spectrum.

Laser ablation followed by electron impact with a low-energy electron beam (5 eV) was also carried out in an attempt to attach electrons to neutral species formed by laser ablation.

Collision-induced dissociation

After formation and trapping of the anions, the anion for study was isolated free of all unwanted anions. This was accomplished by ejecting all the other anions from the cell using a radiofrequency chirp to excite them to orbits in which they collide with the walls of the cell. The target anion remaining in the cell was then excited in the presence of argon at a static pressure of 1×10^{-7} mbar, and after a few collisions the spectrum of the products was observed. The energy involved in the collisions was calculated from the pulse size and duration, the mass and charge of the parent ion and the mass of the target atom. The centre-of-mass energy, that is the energy available for dissociation, was calculated using equations (1) and (2).[15]

$$E_{k(com)} = E_{k(lab)} \frac{m_t}{m_t + m_p} \quad (1)$$

$$E_{k(lab)} = \left(\frac{V_{pp}}{d}\right)^2 \frac{t_{rf}^2 e}{8m_p} \quad (2)$$

Here $E_{k(com)}$ is the centre-of-mass translational kinetic energy (eV), $E_{k(lab)}$ the translational energy imparted to the selected ion by the radiofrequency pulse of t_{rf} seconds duration, V_{pp} the peak-to-peak voltage on the exciter plates, m_t the mass of the collisional atom (Ar), m_p the mass of the selected ion, e the electronic charge, d the diameter of the cylindrical cell and the geometric factor is 0.81.

Collision-induced dissociation experiments were also carried out with carbon tetrachloride as collision gas at a pressure of 1×10^{-7} mbar, using observation of Cl^- to detect electron loss from the selected anion.

Reactions

All unwanted anions were ejected from the cell and the selected ion allowed to react with the gaseous reactant at an uncorrected pressure of 1×10^{-7} mbar. In order to introduce sulfur as reactant gas, the probe tip containing the solid sample was fitted with a capillary tube containing solid sulfur: sulfur gas, S_8, was maintained at an approximately constant pressure of $(1–2) \times 10^{-8}$ mbar by continual vaporisation from the capillary tube.

Results

Ablation of metal sulfides

The impact of the laser pulse on the sample generates local high temperatures, cavities in the solid surface, and a pressure surge due to the vaporised species. Changes of colour in and around the cavities were difficult to observe for the black metal sulfides, but with green MnS there was no colour change at the perimeter

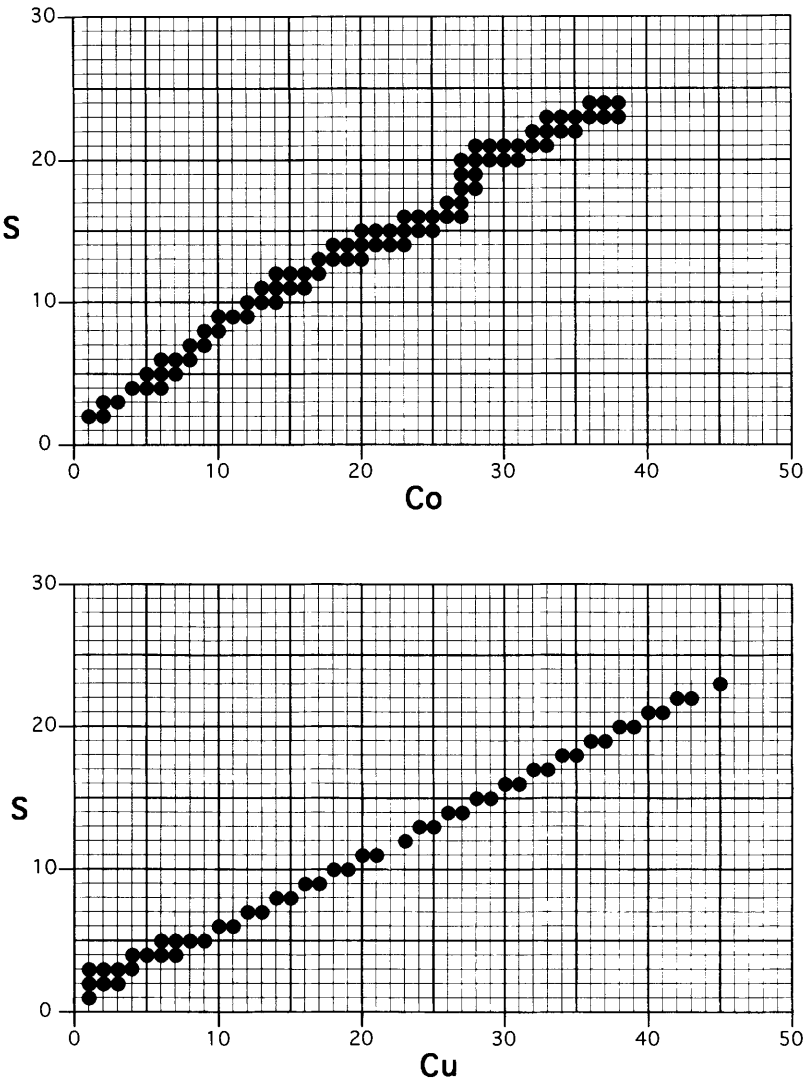

Fig. 1 Maps of the compositions of the observed anions $[Cu_xS_y]^-$ and $[Co_xS_y]^-$. For $[Cu_xS_y]^-$ with $x > 21$ and $[Co_xS_y]^-$ with $x > 22$ the composition could not be confirmed by high-resolution measurements for reasons of insufficient intensity

of the cavity. Often the initial laser pulses produced significant intensities of S_n^- anions, particularly S_3^- which was often the most intense ion in the spectrum. With subsequent pulses the intensity of S_3^- was reduced, and one of the $[M_xS_y]^-$ anions was observed to be the most intense ion. For example, the initial laser pulse on KCu_4S_3 produced a spectrum with the S_3^- most intense and significant intensities for S_2^- and S_4^-. Subsequent pulses resulted in gradual diminution of the S_n^-, and $[CuS_2]^-$ became the most intense anion. In the spectrum of $KFeS_2$, S_3^- was the most intense peak after all laser pulses.

The distributions of observed $[M_xS_y]^-$ anions are shown as maps of *x vs. y*. Fig. 1 shows the anion maps for laser ablation of CuS and CoS, and Fig. 2 shows the anion maps for laser ablation of V_2S_3, Cr_2S_3, MnS, FeS and Ni_3S_2: the ion maps in Fig. 2 also show the relative intensities of the ions. The compositions of the higher-mass ions for Co and Cu in Fig. 1 could not be confirmed by narrow-band or high-resolution measurements because the signals had insufficient intensity, but we are confident of the compositions assigned.

Mixed-metal sulfides

The laser ablation spectra of the mineral Carollite, $CuCo_2S_4$, and of a mixture of copper metal and cobalt sulfide gave principally $[Co_xS_y]^-$ anions with some evidence for less-intense copper anions $[Cu_3S_3]^-$ and $[Cu_5S_4]^-$. The $[Co_3S_3]^-$ anion was the most intense in the spectrum of Carollite. A 1:1 (w/w) mixture of CuS and CoS gave mostly $[Co_xS_y]^-$ anions similar to the distribution from Carollite, with the most intense copper anion at $[Cu_5S_4]^-$. A 5:1 (w/w) mixture of CuS and CoS gave mainly $[Cu_xS_y]^-$ anions with some anions substituted by two Co atoms. The most extensively substituted ions were obtained from a 1:1 mixture of cobalt metal and CuS and a 1:2 mixture of cobalt metal with KCu_4S_3. The broad-band spectrum of cobalt metal with KCu_4S_3 is shown in Fig. 3: $[Co_xS_y]^-$ and $[Cu_xS_y]^-$ anions are abundant and there are significant mixed-metal anions in the $[M_3S_3]^-$ and $[M_5S_4]^-$ regions. Fig. 4 shows the narrow-band spectra of the $[M_5S_4]^-$ and $[M_6S_4]^-$ regions for a mixture of cobalt metal and CuS (1:1 w/w): $[Cu_5S_4]^-$ shows substantial substitution by two cobalt atoms whereas $[Cu_6S_4]^-$ shows less substitution by only one cobalt atom.

Table 1 lists the ions observed on laser ablation of the mixtures of copper sulfides with cobalt metal. The table shows extensive substitution of copper by cobalt for the low-mass ions. The high-mass ions show much less or no substitution of copper by cobalt but a weak, previously unobserved anion $[Cu_{13}S_{10}]^-$ and a highly substituted derivative $[Co_4Cu_9S_{10}]^-$ have been observed from the 1:2 mixture of cobalt metal and KCu_4S_3.

Collision-induced dissociation

Table 2 shows the products of the collisionally induced dissociation of $[Cu_xS_y]^-$ anions with argon, at the centre-of-mass energies listed. Only anions up to $[Cu_{11}S_6]^-$ could be

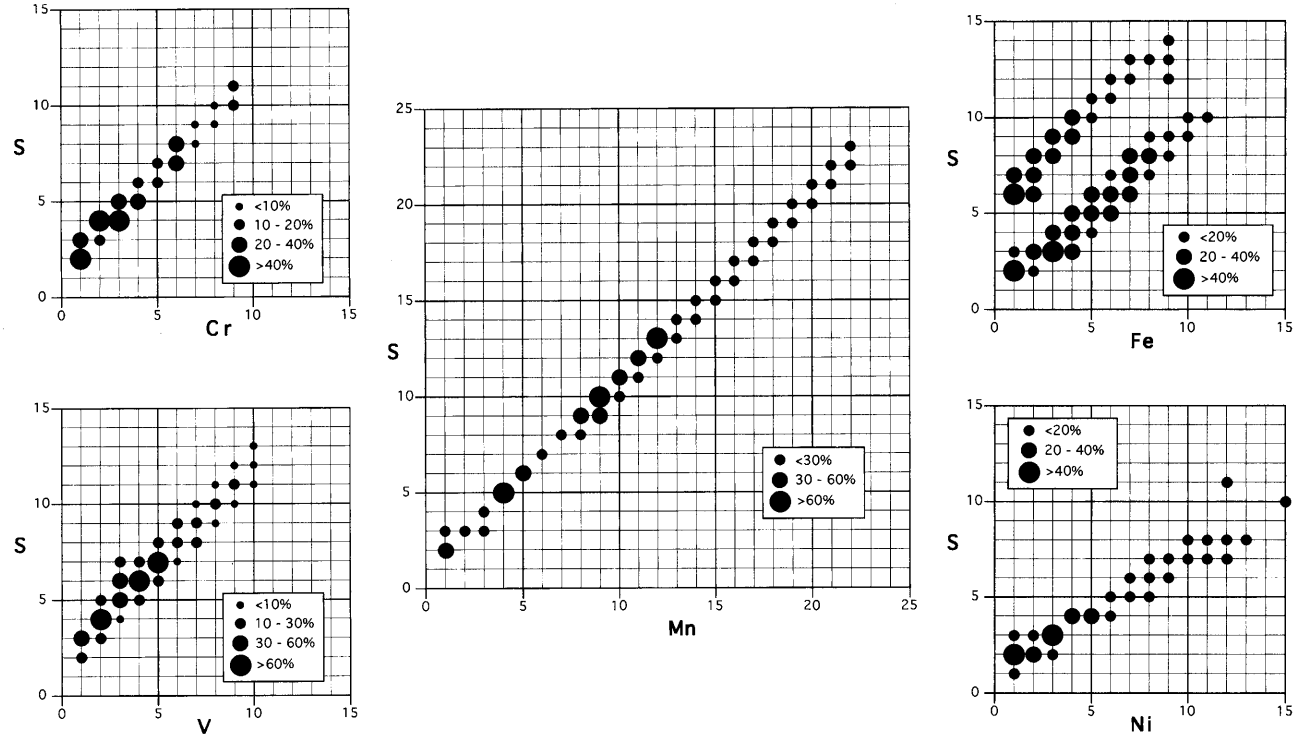

Fig. 2 Maps of the compositions of the $[M_xS_y]^-$ anions formed by laser ablation of V_2S_3, Cr_2S_3, MnS, FeS and Ni_3S_2. The sizes of the circles indicate relative intensities in the mass spectra

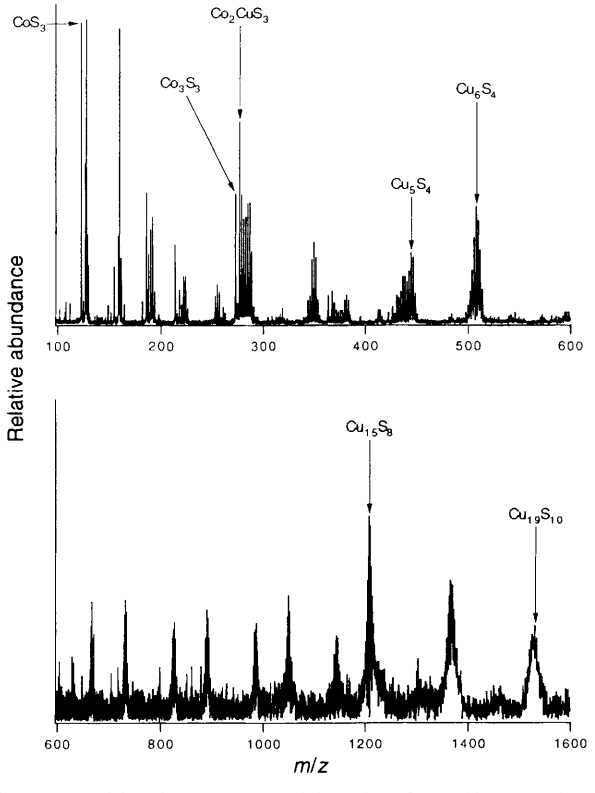

Fig. 3 Broad-band mass spectra of the anions formed by laser ablation of a mixture of cobalt metal and KCu_4S_3 (1:2 w/w). The peak due to completely substituted $[Co_3S_3]^-$ is identified, and the widths of the manifolds in the $[M_3S_3]^-$ and $[M_5S_4]^-$ regions in particular reveal the extent of mixing of Co and Cu in these ions

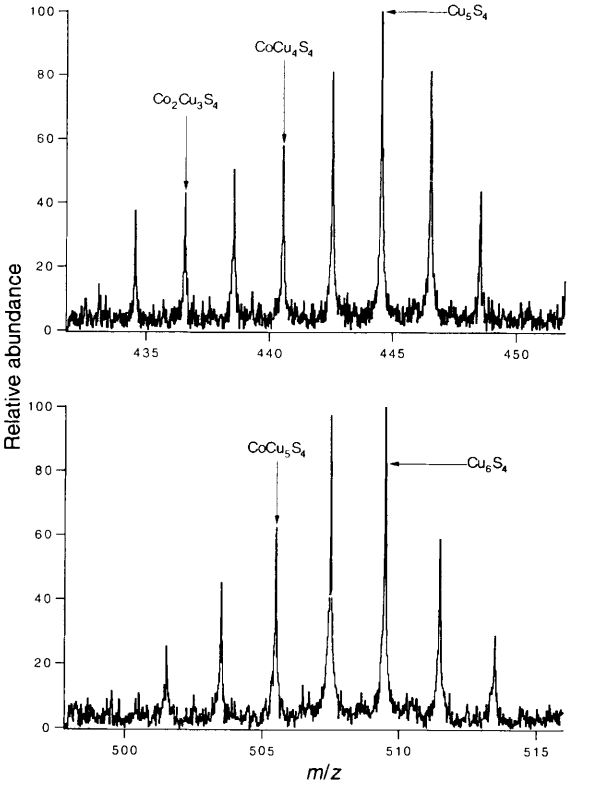

Fig. 4 Narrow-band mass spectra of the $[M_5S_4]^-$ (upper spectrum) and $[M_6S_4]^-$ (lower spectrum) regions for a laser-ablated mixture of cobalt metal and CuS (1:1 w/w). In each case the spectrum is comprised of overlapping isotopomer manifolds, and the peaks containing the most intense member of the manifolds for $[Cu_5S_4]^-$, $[CoCu_4S_4]^-$, $[Co_2Cu_3S_4]^-$, $[Cu_6S_4]^-$ and $[CoCu_5S_4]^-$ are identified

selected cleanly and with sufficient intensity to enable identification of the product ions. The CID results using carbon tetrachloride as collision gas with anions up to and including $[Cu_6S_4]^-$ are shown in Table 3. The chloride ion was observed as a product for five of the $[Cu_xS_y]^-$ anions, signifying electron loss from $[Cu_xS_y]^-$. The centre-of-mass energies for the collisions with CCl_4 are much larger than with argon.

Reactions

Table 4 gives the results of studies of the reactions of selected $[Cu_xS_y]^-$ anions with water, hydrogen sulfide, *n*-propanethiol, benzenethiol and sulfur. The reactions with H_2S, *n*-pro-

Table 1 Mixed-metal sulfide anions observed on laser ablation of mixtures of Co plus CuS, and of Co plus KCu_4S_3

Mass[a]	Most intense anion	Other anions
127	CoS_2	CuS_2
159	CoS_3	CuS_3
190	$CoCuS_2$	Cu_2S_2
224	Cu_2S_3	Co_2S_3, $CoCuS_3$
289	Co_2CuS_3	Cu_3S_3, $CoCu_2S_3$, Co_3S_3
350	Cu_4S_3	$CoCu_3S_3$
382	Cu_4S_4	Co_4S_4, Co_3CuS_4, $Co_2Cu_2S_4$, $CoCu_3S_4$
441	$CoCu_4S_4$	Co_4CuS_4, $Co_3Cu_2S_4$, $Co_2Cu_3S_4$, Cu_5S_4
509	Cu_6S_4	$CoCu_5S_4$
604	Cu_7S_5	$Co_3Cu_4S_5$, $Co_2Cu_5S_5$, $CoCu_6S_5$
667	Cu_8S_5	$CoCu_7S_5$
732	Cu_9S_5	
760	$CoCu_8S_6$	
823	$CoCu_9S_6$	$Co_2Cu_8S_6$, $Cu_{10}S_6$
890	$Cu_{11}S_6$	
922	$Cu_{11}S_7$	$Co_3Cu_8S_7$, $Co_2Cu_9S_7$, $CoCu_{10}S_7$
987	$Cu_{12}S_7$	$Co_2Cu_{10}S_7$, $CoCu_{11}S_7$
1050	$Cu_{13}S_7$	
1146	$Cu_{13}S_{10}$[b]	$Co_4Cu_9S_{10}$
1210	$Cu_{15}S_8$	
1367	$Cu_{17}S_9$	
1527	$Cu_{19}S_{10}$	

[a] Mass of the most intense peak of the manifold of isotopomers of overlapping ions. [b] Previously unidentified ion in the mass spectra of pure copper sulfides.

Table 2 Collision-induced dissociation of $[Cu_xS_y]^-$ anions with argon

Parent anion	E_{com}*/eV	Product anions
Cu_2S_2	108	CuS_2, CuS
Cu_2S_3	82	S_2
Cu_3S_2	66	Cu_2S_2, S_2
Cu_3S_3	96	S_2
Cu_4S_3	38	Cu_3S_3, S_2
Cu_4S_4	59	Cu_3S_3, S_2
Cu_5S_4	48	Cu_4S_4, Cu_4S_3, Cu_3S_3, S_2
Cu_6S_4	56	Cu_5S_4, Cu_4S_3, S_2
Cu_8S_5	22	Cu_6S_4
Cu_9S_5	15	Cu_8S_5, Cu_6S_4
$Cu_{10}S_6$	15	Cu_9S_5, Cu_8S_5, Cu_6S_4
$Cu_{11}S_6$	13	$Cu_{10}S_6$, Cu_9S_5, Cu_8S_5, Cu_6S_4

* Centre-of-mass energy of the collisions of the anions with argon at 1×10^{-7} mbar.

Table 3 Collision-induced dissociation of $[Cu_xS_y]^-$ anions with carbon tetrachloride

Parent anion	E_{com}*/eV	Product anions
Cu_2S_2	279	CuS_2, CuS, S_2, Cl
Cu_2S_3	222	S_2, Cl
Cu_3S_2	188	S_2, Cl
Cu_3S_3	155	S_2, Cl
Cu_4S_3	114	S_2, Cu_3S_3
Cu_4S_4	101	S_2, Cl
Cu_5S_4	85	S_2, Cu_4S_4
Cu_6S_4	114	Cu_4S_4

* Centre-of-mass energy of the collisions of $[Cu_xS_y]^-$ anions with carbon tetrachloride at 1×10^{-7} mbar.

panethiol and benzenethiol were at an uncorrected gauge pressure of 1×10^{-7} mbar. In general the smaller anions were more reactive than the larger anions. Fig. 5 shows the reaction products of $[Cu_5S_4]^-$ and $[Cu_6S_4]^-$ anions with H_2S. Note that in the relatively long reaction period of 20 s there is major conversion of $[Cu_5S_4]^-$ into $[Cu_5S_4{\cdot}H_2S]^-$ but minor conversion of $[Cu_6S_4]^-$ into $[Cu_6S_4{\cdot}H_2S]^-$. Besides the products with added H_2S, there are some ions formed by dissociation. Further, the anion HS^- was a minor product in

Table 4 Reactions of $[Cu_xS_y]^-$ anions

Selected anion	H_2O	H_2S	Pr^nSH	PhSH	S_8[a]
Cu_2S_2	Add ($+O_2$)	Add[b]	+S	Add	S_2, S_4 (S_5, S_6)
Cu_2S_3	n.r.[c]	Add	Add	Add	S_6
Cu_3S_3	n.r.	n.r.	n.r.	n.r.	S_6, (S_4, S_5)
Cu_4S_3	Add	Add	+S	Add	S_4, S_5
Cu_4S_4	n.r.	Add	Add	Add	S_6
Cu_5S_4	n.r.	Add	Add	Add	S_6
Cu_6S_4	n.r.	Add	Add	Add	n.r.
Cu_8S_5	n.r.	n.r.	n.r.	Add	S_4
Cu_9S_5	n.r.	n.r.	n.r.	n.r.	S, S_2, S_3
$Cu_{10}S_6$	n.r.	n.r.	n.r.	n.r.	n.r.
$Cu_{11}S_6$	n.r.	n.r.	n.r.	n.r.	S_2

[a] Addition of S_n to the selected ion; minor products in parentheses. [b] Add = Addition of one molecule. [c] n.r. = No reaction.

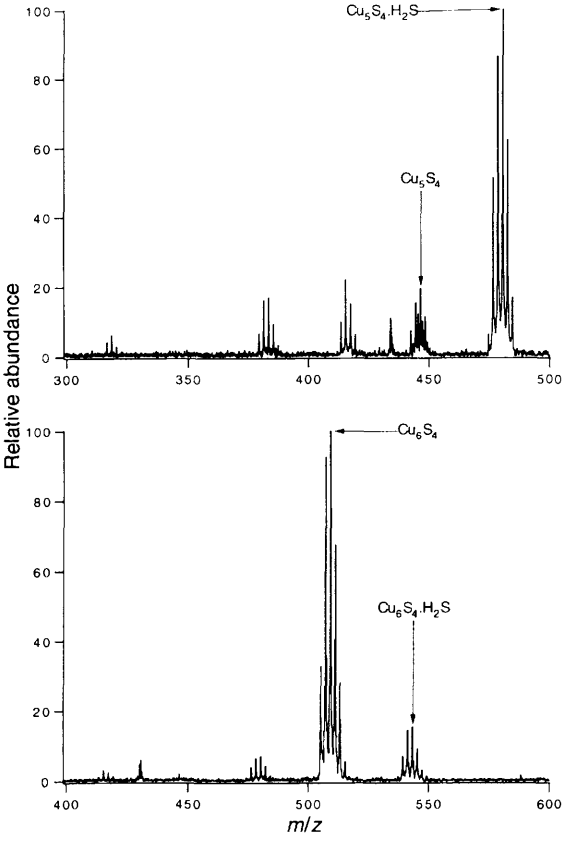

Fig. 5 Mass spectra showing the isotopomer manifolds for the products of reaction of selected anions $[Cu_5S_4]^-$ (upper spectrum) and $[Cu_6S_4]^-$ (lower spectrum) with H_2S at 1×10^{-7} mbar for 20 s

the reactions of all $[Cu_xS_y]^-$ anions up to $[Cu_6S_4]^-$ with the exception of $[Cu_3S_3]^-$: the formation of HS^- is evidence of protonation of the $[Cu_xS_y]^-$ anion. Fig. 6 shows the reaction of $[Cu_8S_5]^-$ with sulfur vapour. Table 4 indicates that most $[Cu_xS_y]^-$ anions are reactive towards sulfur with the exceptions of $[Cu_6S_4]^-$ and $[Cu_{10}S_6]^-$. It is noticeable that the smaller anions add S_6 or S_4 units whereas the larger ions add S or S_2 units.

Discussion

Anion formation

The mechanism of anion formation by laser ablation is as yet poorly understood, but our experiments show that the $[M_xS_y]^-$ anions are not simply fragments excised from the metal sulfide lattice. The formation of mixed-metal molecular clusters from

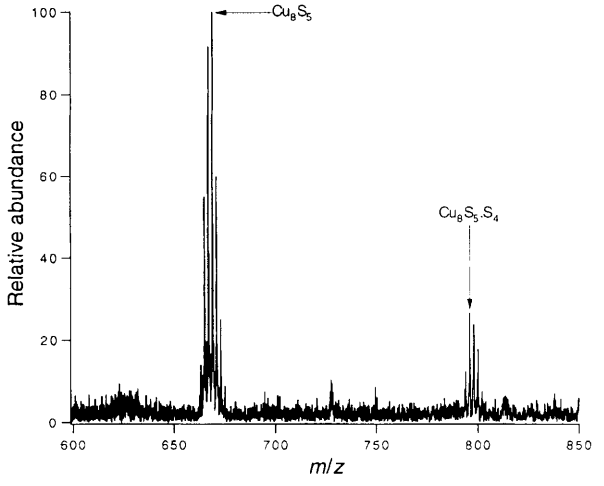

Fig. 6 Mass spectrum of the reaction of $[Cu_8S_5]^-$ with S_8 vapour [(1–2) × 10^{-8} mbar] for 20 s

physical mixtures of cobalt with copper sulfide, and the formation of copper selenide and telluride anions from mixtures of copper with selenium or tellurium,[4] confirm that the clusters observed must be assembled in the gas phase.

In general the most intense anions in the spectra occur in the lower-mass ranges, but there are significant exceptions such as the copper species in the vicinity of $[Cu_{29}S_{15}]^-$, and $[Mn_{12}S_{13}]^-$ is the most intense anion in the MnS mass spectrum. There are unanswered questions about the formation processes for the anions observed. They could be formed in the early stages after laser ablation or in the cooling laser plume. They could be formed as anions, or as neutral species, of which those with the highest electron affinities capture the low-energy electrons.

The ion maps show fairly narrow distributions of composition for the $[M_xS_y]^-$ anions, and it is significant that there are large regions where possible metal sulfide anions are not observed. One interpretation of this is that the observed ions are those with the more favourable electron affinities amongst wider distributions of neutral clusters. Experiments designed to detect such neutral $[M_xS_y]$ species produced by the ablation process used electron impact (5 eV) immediately after laser ablation, with the expectation that any neutral clusters would become evident as observable anions. However these experiments resulted only in increases in the intensities of the S_n anions, and no new metal sulfide anions. This suggests that if neutral species with compositions differing from those of the regions of the observed anions exist, they are not stable as anions, or they do not have high enough electron affinities in the competition to form anions.

We believe that the distributions on the ion maps reveal the regions of stability, specifically thermodynamic, kinetic, and electronic stability, for $[M_xS_y]$ molecules. This interpretation is supported also by the fact that the compositions of the anions observed from the laser ablation of the metal sulfides are related to the position of the metal in the transition-metal series. Thus vanadium early in the transition period forms ions with a sulfur to vanadium ratio greater than 1:1, whereas the copper to sulfur ratio is almost 2:1 in the higher-mass copper sulfide anions. This point is discussed further below with the electron populations.

The ion maps also show some other interesting features. The map for $[Fe_xS_y]^-$ shows two different sets of anions, one with $y \approx x$ and the other with $y \approx x + 5$. All of the iron sulfides examined produce relatively large amounts of free sulfur on ablation (compared to copper sulfides) and S_3^- is the most intense anion in the spectra. It could be that the $[Fe_xS_y]^-$ anions where $y \approx x$ react with the free sulfur molecules in the gas phase to produce the second set of ions. This possibility, supported by the S_n addition reactions for copper listed in Table 4, is under investigation. The ion map for cobalt shows some non-linear behaviour in the region of 20–30 cobalt atoms which may indicate a change in the structure of the anions at this size. The highest-mass anions tend to have a higher cobalt to sulfur ratio than do the lower-mass anions, which suggests the growth of an inner core of metal atoms.

The experiments with mixed precursors show some interesting results. When cobalt and copper are in competition, the cobalt sulfide anions are generally formed in preference to copper–sulfur anions. The formation of mixed cobalt–copper–sulfur anions (and the pure cobalt–sulfur anions) when cobalt metal is mixed with the copper sulfides confirms again that the processes leading to the final products must involve dissociation and reassociation of the components of the solid precursors. The replacement of copper by cobalt appears to be extensive in the low-mass region, where the copper to sulfur ratio deviates from 2:1, but much less so in the larger products where the ratio approaches 2:1. Thus some small stable copper and cobalt anions have the same formulae, *e.g.* $[M_3S_3]$, and Fig. 3 shows the extent of substitution in these anions. In general we are observing mixed-metal cluster anions mainly in regions where the compositions of the single metal clusters are not markedly different. The replacements of a single Cu by Co in $[M_9S_6]^-$ and $[M_{10}S_6]^-$ do involve cluster compositions which are not observed for Co alone. The small amount of occurrence of a single Co in $[Cu_6S_4]^-$ is again evidence for the stability of $[Cu_6S_4]^-$. Other significant results are the formation of the new anion $[Cu_{13}S_{10}]^-$ and the highly substituted anion $[Co_4Cu_9S_{10}]^-$ from mixtures of cobalt metal with KCu_4S_3. Investigations of other mixtures of transition metals with metal sulfides are currently in progress.

Electron populations

The dependence of the slopes of the distributions in the ion maps on the atomic number of the transition metal suggests that electron populations influence the compositions of the $[M_xS_y]^-$ clusters. We have evaluated the number of bonding electrons in each cluster, normalised by the number of metal atoms. Thus the electron number N_m is the sum of the number of 3d and 4s electrons for the (neutral) metal atoms, plus six electrons for each sulfur atom, plus one electron due to the charge of the ion, all divided by the number of metal atoms. Table 5 shows selected values of N_m, allowing comparison of clusters with the same numbers of metal atoms for Groups 5–11 of the Periodic Table. The most obvious point is that the N_m values are all in the range 12–16. Within each group the larger values of N_m occur for the smaller clusters, and as the cluster size increases the values slowly approach 12.

It is remarkable that even though the compositions and consequently the structures of the $[M_xS_y]^-$ anionic molecules change quite drastically through the transition series for any value of x, the electron populations N_m are essentially constant (there is a very small secondary increase in N_m values from left to right). This implies that even though there must be considerable diversity in the actual geometrical structures for the 290 clusters on the ion maps, they all follow one overall bonding principle controlling the number of electrons involved. Alternatively stated, metal atoms low in electrons accommodate more sulfur atoms, while electron-rich metal atoms use relatively few sulfur atoms. Thus, for example, V_{10} associates with S_{12}, Mn_{10} with S_{11}, Fe_{10} with S_9, Co_{10} with S_8, Ni_{10} with S_7 and Cu_{10} with S_6. We regard the constancy of N_m as further evidence that our experiments are generally yielding stable metal sulfide anions.

This property N_m of the metal sulfide clusters has fundamental predictive value. Prior to our laser-ablation investigations, prediction of the compositions of transition-

Table 5 Valence electron populations per metal atom, N_m, in $[M_xS_y]^-$ anions

Ion	V		Cr		Mn		Fe		Co		Ni		Cu	
M_xS_y	Ion	N_m	Ion	N_m	Ion	N_m	Ion	N_m	Ion	N_m	Ion	N_m	Ion	N_m
M_4S_y	V_4S_6	14.3	Cr_4S_5	13.8	Mn_4S_5	14.8	Fe_4S_4	14.3	Co_4S_4	15.3	Ni_4S_4	16.3	Cu_4S_3	15.8
M_6S_y	V_6S_8	13.2	Cr_6S_7	13.2	Mn_6S_7	14.2	Fe_6S_7	15.2	Co_6S_6	15.2	Ni_6S_4	14.0	Cu_6S_4	15.0
M_9S_y	V_9S_{11}	12.4	Cr_9S_{11}	13.4	Mn_9S_{10}	13.8	Fe_9S_9	14.1	Co_9S_8	14.4	Ni_9S_6	14.1	Cu_9S_5	14.4
$M_{10}S_y$	$V_{10}S_{12}$	12.3			$Mn_{10}S_{11}$	13.7	$Fe_{10}S_9$	13.5	$Co_{10}S_8$	13.9	$Ni_{10}S_7$	14.3	$Cu_{10}S_6$	14.7
$M_{15}S_y$					$Mn_{15}S_{15}$	13.1			$Co_{15}S_{12}$	13.8	$Ni_{15}S_{10}$	14.1	$Cu_{15}S_8$	14.3
$M_{19}S_y$					$Mn_{19}S_{19}$	13.1			$Co_{19}S_{13}$	13.2			$Cu_{19}S_{10}$	14.2
$M_{22}S_y$					$Mn_{22}S_{23}$	13.3			$Co_{22}S_{14}$	12.9			$Cu_{22}S_{12}$	14.3
$M_{23}S_y$									$Co_{23}S_{16}$	13.2			$Cu_{23}S_{12}$	14.2
$M_{37}S_y$									$Co_{37}S_{24}$	12.9			$Cu_{37}S_{19}$	12.1

For $[M_xS_y]^-$, $N_m = [x(\text{number of 3d and 4s electrons in } M^0) + 6y + 1]/x$.

metal sulfide molecules would have been difficult, possibly based on the concepts of metal oxidation state, and probably wrong. The primary constancy of N_m, and its minor variations discussed in the previous paragraph, allow prediction with confidence of the compositions of metal sulfide molecules. Thus, although molecular titanium sulfides are not yet known, we can predict, for example, that the monoanionic clusters with 15 Ti atoms will most likely contain 21 and 22 S atoms.

The small variations in N_m values could well reflect variations in the bonding networks and thus the involvement of metal and sulfur electrons. An assumption in the calculation of N_m is that all M and S atoms are connected isotropically to other atoms. However surface atoms, M and/or S, could possess orbitals and electrons which are essentially non-bonding, and less likely to conform to the general pattern. It must also be remembered that for the smaller clusters the integral numbers of atoms reduce the precision and significance of the calculation. Nevertheless, the constancy of the N_m values in Table 5 for Mn_9S_{10} through $Mn_{22}S_{23}$, for $Co_{10}S_8$ through $Co_{37}S_{24}$, and for Cu_9S_5 through $Cu_{23}S_{12}$, is impressive.

More detailed interpretation of the bonding and electron populations in these metal sulfide cluster anions will come from applications of density functional theory (see below).

Collision-induced dissociation

Acceleration of the copper–sulfur anions and collision with argon does result in dissociation, but the high centre-of-mass energies required attest to the stability of these anions. In similar CID experiments with copper oxide anions Freiser and co-workers[12] used much lower centre-of-mass energies to obtain considerable dissociation of the anions. For example, the anion $[Cu_5O_4]^-$ was greater than 90% dissociated with a centre-of-mass energy of 14 eV whereas the anion $[Cu_5S_4]^-$ was less than 50% dissociated with a centre-of-mass energy of 48 eV. Similarly positive ions[16] in the series $[FeS_y]^+$ where y = 2–6 were considerably dissociated in argon with $E_{com} \approx 10$ eV. This shows the relatively high stability of the copper sulfide clusters. The loss of Cu or CuS neutral species is a common process, as is the formation of S_2^-, $[Cu_3S_3]^-$ and $[Cu_6S_4]^-$ anions. The ion $[Cu_6S_4]^-$ appears commonly as a product of the dissociation of the higher-mass ions, while S_2^- and $[Cu_3S_3]^-$ appear as products of the dissociation of the lower-mass ions. This indicates that the $[Cu_3S_3]^-$ and $[Cu_6S_4]^-$ anions are relatively more stable than the others.

Collision-induced dissociation experiments often involve loss of signal intensity of the ions. One possible cause is electron detachment during the collision. This process cannot be detected using argon as collision gas, but carbon tetrachloride has been used in photodetachment experiments to collect low-energy electrons and give the chloride ion in an ICR trap.[17] The electrons lost during photodetachment experiments react with carbon tetrachloride and form Cl^-. We have now used this method to observe electron loss during translationally excited collisions. Several of the ions studied gave no Cl^- on collision-induced dissociation, and so the detection of Cl^- is evidence of electron detachment. Electron detachment does occur for the low-mass copper sulfide anions but does not occur for the higher-mass ions. With both $[Cu_3S_3]^-$ and $[Cu_4S_4]^-$ anions the formation of Cl^- is not substantial and electron detachment for these ions may be considered a minor pathway. As shown by N_m, the small ions are relatively electron rich and so might lose an electron more easily than the electron-poor high-mass anions.

Reactions

The copper sulfide anions are not reactive with CO, N_2O, benzene, acetone or alcohols ROH (R = Me, Et or Pr^i) at 1×10^{-7} mbar. Only two $[Cu_xS_y]^-$ react with water at a similar pressure: $[Cu_2S_2]^-$ gives two products, addition of one water molecule $[Cu_2S_2{\cdot}H_2O]^-$, and an ion of mass 32 larger than Cu_2S_2. The ion $[Cu_2S_2]^-$ reacts with sulfur vapour by the addition of two or more sulfur atoms. We ascribe the additional mass of 32 in the reaction with water to two O atoms rather than one S atom, giving the anion $[Cu_2S_2O_2]^-$ from $[Cu_2S_2]^-$ + H_2O. The ion $[Cu_4S_3]^-$ also adds one water molecule but there is no evidence for the addition of mass 32 to $[Cu_4S_3]^-$. The ions $[Cu_2S_2]^-$ and $[Cu_4S_3]^-$ are the most reactive copper sulfide anions. Most of the lower-mass anions react with sulfur compounds by the addition of one molecule of reactant [equation (3)] but the higher-mass ions often do not react

$$[Cu_xS_y]^- + RSH \longrightarrow [Cu_xS_y{\cdot}RSH]^- \qquad (3)$$

or react very slowly. Benzenethiol reacts faster than *n*-propanethiol with all the anions, and proton abstraction [equation (4)] to form the RS^- anion is a minor reaction

$$[Cu_xS_y]^- + RSH \longrightarrow Cu_xS_yH + RS^- \qquad (4)$$

pathway for H_2S, *n*-propanethiol and benzenethiol. The anion $[Cu_3S_3]^-$ is unreactive towards the thiols and H_2S and $[Cu_6S_4]^-$ is much less reactive (and shows less dissociation) than the other anions, as shown for H_2S in Fig. 6.

The reactions of the anions with sulfur are intriguing. The low-mass ions react by addition of principally S_4 and S_6 whereas the high-mass ions react by the addition of one or two sulfur atoms. The molecular S_4 and S_6 could act as simple cyclic ligands or as several S_2 ligands; the former seems most likely as no intermediate S_2 addition is observed in the addition of S_6 and S_7 to $[Cu_5S_4]^-$. Similarly Fig. 6 does not show addition of S_2 to the anion $[Cu_8S_5]^-$, only addition of S_4. There are known clusters (characterised in crystals) which are similar and have polysulfide ligands co-ordinating a copper cluster, such as

$[Cu_6(S_4)_3S_5]^{2-}$ (refs. 18 and 19) and $[\{Cu_4(S_4)(S_5)_2\}_{0.4}\{Cu_4(S_5)_3\}_{0.6}]^{2-}$.[20]

Structures

Essential questions arise about the geometrical and electronic structures of our clusters. The mass spectrometric characterisation yields little information about their structure, and spectroscopic data are not yet available. Even with full availability of spectroscopic data it is unlikely that the multiple structural possibilities for clusters containing more than about five metal atoms could be resolved unambiguously. Further, it is expected that the geometry/energy hypersurfaces will become increasingly soft as the cluster size increases.

In this context density functional (DF) theory is a very attractive computational method for advancing the understanding of structure. The key advantage of DF methodology for large molecules and molecules with large atoms is its incorporation of electron correlation while maintaining computational expediency. Our density functional calculations, with the program DMOL,[21] use the Lee–Yang–Parr[22] and Becke[23] functionals which incorporate gradient corrections, and use double numerical basis sets including polarisation functions. Our initial goals are to paint the broad-brush picture of the geometry/energy surface for each cluster, and to recognise the key structural principles and the favourable and unfavourable characteristics of metal chalcogenide molecular architecture. To develop this initial picture, we postulate structures, optimise their geometries without imposition of the maximum symmetry and compare energies. In developing postulated structures we incorporate the structural principles which are evident from any related terminally ligated clusters in crystals.[1] When the principal energy wells in the geometry/energy surfaces are located, we can investigate finer details of electronic structure, spin states and reactivities.

In the following discussion we concentrate on copper chalcogenide clusters. It is most significant that the composition pattern we observe in the gas phase, namely $[Cu_{2x-1}E_x]^-$, is virtually the same as that of the cores of the amazing clusters $Cu_{2x}E_x(PR_3)_p$ (E mainly Se; x = 15, 18, 22, 35 or 73) prepared and characterised crystallographically by Fenske and co-workers.[24–26] In both series the Cu atoms are formally electron-precise Cu^I. Thus the Fenske structures can be used as models for our clusters, which constitute the complete sequence for x up to 23.

The most abundant of the high-mass $[Cu_{2x-1}S_x]^-$ clusters is $[Cu_{29}S_{15}]^-$, for which Fenske's characterised cluster $[Cu_{29}Se_{15}(PPr^i_3)_{12}]$ {closely related to $[Cu_{30}Se_{15}(PPr^i_3)_{12}]$[24]} provides a pertinent model. In a test of the accuracy of our computational method, optimisation of the geometry of $[Cu_{29}Se_{15}(PH_3)_{12}]$ yielded bond distances which are within *ca.* 0.05 Å of those measured. Ahlrichs and co-workers[27–29] report that Hartree–Fock calculations including dynamic electron correlation yield very good descriptions of $[Cu_{2x}Se_x]$ and $[Cu_{2x}Se_x(PR_3)_m]$ clusters for $x \leqslant 6$ and R = H or CH_3.

The geometry of the core of $[Cu_{29}Se_{15}(PPr^i_3)_{12}]$ provides a starting point for optimisation of the structure of $[Cu_{29}S_{15}]^-$, which reveals (see Fig. 7) that two Cu atoms at the ends of the three-fold axis in $[Cu_{29}Se_{15}(PPr^i_3)_{12}]$ move inside the copper core of $[Cu_{29}S_{15}]^-$, while the Cu_3 triangle at the centre of the cluster undergoes contraction.

The geometrical principles for $[Cu_xS_y]^-$ clusters are revealed by investigation of smaller instances. In particular, $[Cu_3S_3]^-$ and $[Cu_6S_4]^-$ are more abundant and less reactive than their neighbours, implying special stability. The results of density functional calculations on the isomers of these structures are shown in Figs. 8 and 9. The most stable structure for $[Cu_3S_3]^-$ is the planar triangular array $Cu_3(\mu\text{-}S)_3$, **A**. Introduction of triply bridging sulfide, as in $Cu_3(\mu\text{-}S)_2(\mu_3\text{-}S)$ **B**, decreases the stability (*i.e.* the binding energy is less negative) by *ca.* 150 kJ mol^{-1}, and structure **B** optimises to **A**. For $[Cu_6S_4]^-$ the most stable structure is **C**, octahedro-Cu_6-tetrahedro-$(\mu_3\text{-}S)_4$, with idealised symmetry T_d. The alternative postulate **D** (C_{2v}), in which a trigonal prism of Cu is capped $(\mu_4\text{-}S)_2(\mu_3\text{-}S)_2$, is less stable by *ca.* 200 kJ mol^{-1} and is not an energy minimum, optimising (in point group C_2) to **E** (C_{2v}) at an energy of +159 kJ mol^{-1} relative to **C**. Structure **F**, with the same connectivity as **D** and **E**, has an energy of +142 kJ mol^{-1} relative to **C**. All other postulates for $[Cu_6S_4]^-$ are substantially less stable.

It is significant that the most stable structures for both

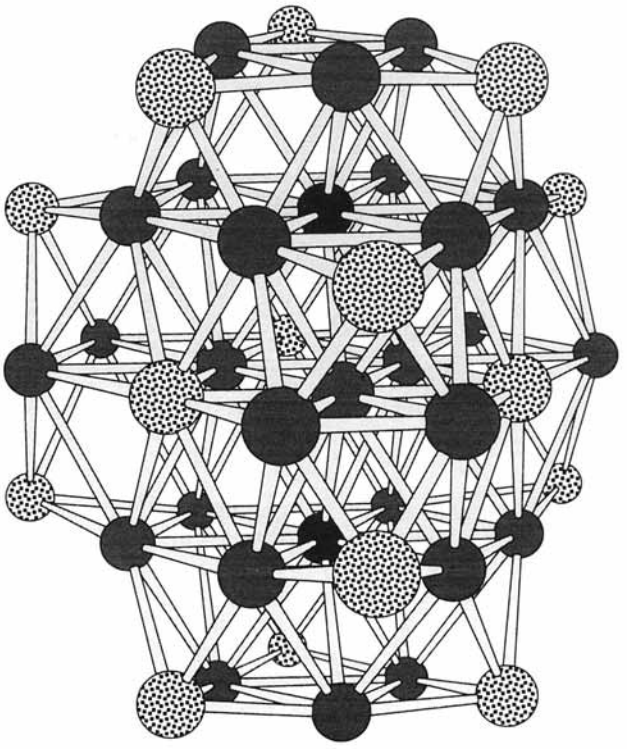

Fig. 7 The optimised structure of $[Cu_{29}S_{15}]^-$, based on the structure of $[Cu_{29}Se_{15}(PPr^i_3)_{12}]$. Sulfur atoms are stippled. The two Cu atoms at the centres of the upper and lower Cu_6 hexagons have moved into the core of the structure, and the central triangle of Cu atoms between the black Cu atoms has contracted

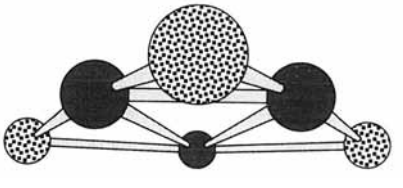

A

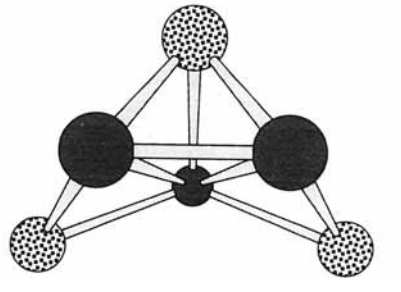

B

Fig. 8 Structures for $[Cu_3S_3]^-$ (sulfur atoms are stippled): **A**, with $(\mu\text{-}S)_3$ is *ca.* 150 kJ mol^{-1} more stable than **B**, reflecting the stabilising effect of pseudo-linear S–Cu–S local co-ordination

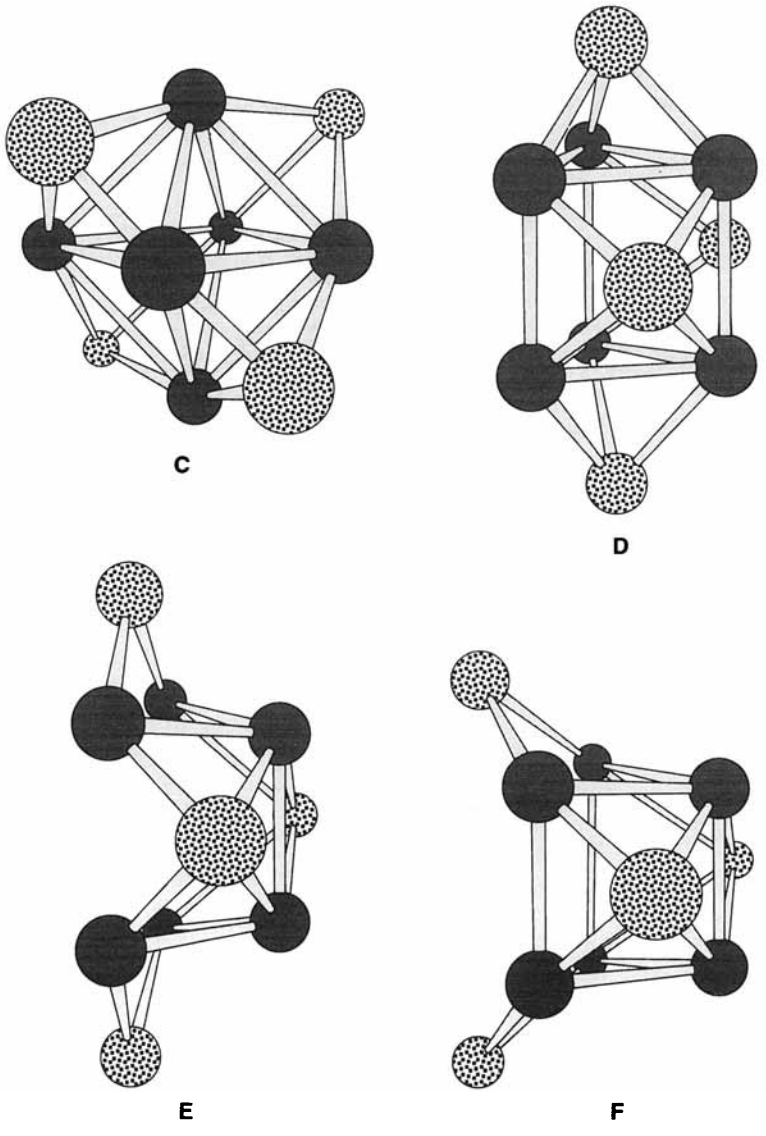

Fig. 9 Structures for $[Cu_6S_4]^-$ (sulfur atoms are stippled): **C** is more stable by at least 140 kJ mol^{-1} than any other structure, **D** optimises to **E** and **F** is more stable than **E** by 17 kJ mol^{-1}

$[Cu_3S_3]^-$ and $[Cu_6S_4]^-$ are those which allow the maximum number of Cu atoms to adopt local CuS_2 co-ordination as pseudo-linear (angles 165 ± 10°). Thus Cu_3S_3 **A** is effectively comprised of three linear S–Cu–S moieties, while Cu_6S_4 **C** has six linear S–Cu–S moieties along the edges of a tetrahedron (and the second most stable structure **F** contains four S–Cu–S moieties with 155° angles). This geometrical feature of stable clusters is not surprising, and has been noted also by Schafer and Ahlrichs[29] for $Cu_{2x}Se_x$ clusters. Our results demonstrate the relationship between this local favourable co-ordination of Cu atoms and their lack of further reactivity. In this context it is notable that $[CuS_2]^-$ is the most abundant species in our mass spectrum. Another structural principle which is becoming apparent for Cu_xE_y clusters is that trigonal local CuE_3 co-ordination is also a stabilising feature: $[CuS_3]^-$ is the second most abundant species in our mass spectrum.

These structural principles can be combined with reactivity data to guide the postulation of structures for other and larger $[Cu_{2x-1}S_x]^-$ clusters. Table 4 reveals that $[Cu_{10}S_6]^-$ is the least reactive of those investigated. Using our postulated principles, this is interpreted as evidence that there is no exposed Cu atom with co-ordination other than pseudo-linear CuS_2 or pseudo-trigonal CuS_3. Fig. 10 shows a postulated structure, **G**, which fulfils these requirements for $[Cu_{10}S_6]^-$. Note that it contains two Cu_3S_3 **A** moieties.

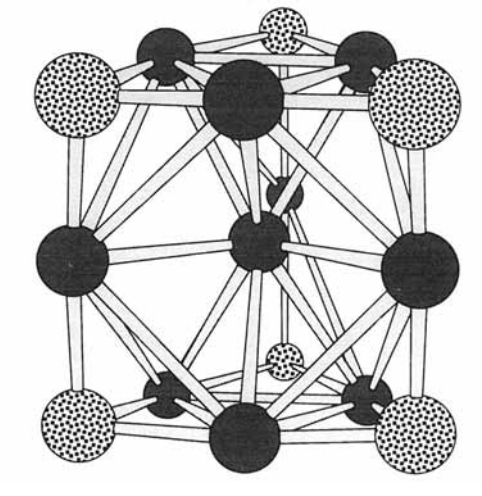

Fig. 10 The symmetrical structure **G** postulated for $[Cu_{10}S_6]^-$

Conclusion

We have demonstrated the value of an investigative approach to binary molecular clusters which combines (*a*) generation by

laser ablation, (*b*) characterisation of stability and reactivity by FTICR and (*c*) DF computation of electronic and geometrical structure. These investigations are informed by comparison with relevant clusters characterised in crystals, but it is also clear that gas-phase metal sulfide clusters have a distinctive and fundamental chemistry of their own. A separate publication will contain details of the reactions of the $[Cu_{2x-1}S_x]^-$ clusters, and full details of the optimised geometries and electronic structures of other members of the series.

References

1 I. G. Dance and K. J. Fisher, *Prog. Inorg. Chem.*, 1994, **41**, 637.
2 J. El Nakat, K. J. Fisher, I. G. Dance and G. D. Willett, *J. Chem. Soc., Chem. Commun.*, 1991, 746.
3 J. El Nakat, K. J. Fisher, I. G. Dance, G. D. Willett and D. Rice, *J. Am. Chem. Soc.*, 1991, **113**, 5141.
4 I. G. Dance, K. J. Fisher, J. El Nakat and G. D. Willett, *Inorg. Chem.*, 1991, **30**, 2957.
5 J. El Nakat, K. J. Fisher, I. G. Dance and G. D. Willett, *Inorg. Chem.*, 1993, **32**, 1931.
6 I. G. Dance and K. J. Fisher, *Mater. Sci. Forum*, 1994, **152–153**, 137.
7 T. Hong Lee and K. M. Ervin, *J. Phys. Chem.*, 1994, **98**, 10 023.
8 L. Sallans, K. R. Lane, R. R. Squires and B. S. Freiser, *J. Am. Chem. Soc.*, 1985, **107**, 4379.
9 L. Sallans, K. R. Lane and B. S. Freiser, *J. Am. Chem. Soc.*, 1989, **111**, 865.
10 W.-L. Lee, D. A. Gage, Z.-H. Huang, C. K. Chang, M. G. Kanatzidis and J. Allison, *J. Am. Chem. Soc.*, 1992, **114**, 7132.
11 H. Feld, A. Leute, D. Rading, A. Benninghoven, G. Henkel, T. Kruger and B. Krebs, *Z. Naturforsch., Teil B*, 1992, **47**, 929.
12 J. R. Gord, R. J. Bemish and B. S. Freiser, *Int. J. Mass Spectrom. Ion Processes*, 1990, **102**, 115.
13 S. W. McElvany, *Int. J. Mass Spectrom. Ion Processes*, 1990, **102**, 81.
14 I. G. Dance, P. A. W. Dean and K. J. Fisher, *Inorg. Chem.*, 1994, **33**, 6261.
15 C. E. C. A. Hop, T. B. McMahon and G. D. Willett, *Int. J. Mass Spectrom. Ion Processes*, 1990, **101**, 191.
16 T. J. MacMahon, T. C. Jackson and B. S. Freiser, *J. Am. Chem. Soc.*, 1989, **111**, 421.
17 B. Pozniak and R. C. Dunbar, *Int. J. Mass Spectrom. Ion Phys.*, 1994, **133**, 97.
18 G. Henkel, P. Betz and B. Krebs, *J. Chem. Soc., Chem. Commun.*, 1984, 314.
19 A. Müller, M. Römer, H. Bögge, E. Krickemeyer, and D. Bergmann, *Z. Anorg. Allg. Chem.*, 1984, **511**, 84.
20 A. Müller, M. Römer, H. Bögge, E. Krickmeyer and K. Schmitz, *Inorg. Chim. Acta*, 1984, **85**, L39.
21 Biosym Technologies, Inc., San Diego, CA, v2.3 and v2.36; see B. Delley, M. Wrinn, and H. P. Lüthi, *J. Chem. Phys.*, 1994, **100**, 5785.
22 C. Lee, W. Yang and R. G. Parr, *Phys. Rev. B*, 1988, **37**, 785.
23 A. D. Becke, *Phys. Rev. A*, 1988, **38**, 3098.
24 D. Fenske, H. Krautscheid and S. Balter, *Angew. Chem., Int. Ed. Engl.*, 1990, **29**, 796.
25 D. Fenske and H. Krautscheid, *Angew. Chem., Int. Ed. Engl.*, 1990, **29**, 1452.
26 S. Dehnen and D. Fenske, *Angew. Chem., Int. Ed. Engl.*, 1994, **33**, 2287.
27 A. Schafer, C. Huber, J. Gauss and R. Ahlrichs, *Theor. Chim. Acta*, 1993, **87**, 29.
28 S. Dehnen, A. Schafer, D. Fenske and R. Ahlrichs, *Angew. Chem., Int. Ed. Engl.*, 1994, **33**, 746.
29 A. Schafer and R. Ahlrichs, *J. Am. Chem. Soc.*, 1994, **116**, 10 686.

Received 31*st July* 1995; *Paper* 5/06037K